Supporting Information

Construction of high-nuclear 4p-4f heterometallic $\{Ln_{11}Ge_{12}\}$ cluster-organic frameworks with high-sensitivity luminescent sensing of Fe^{3+} in aqueous solution

Leilei Li,[a] Bin Cai,[b] Donghui Pang,[a] Xinxin Du,[a] Xingliang Yin,[a] Huaiwei Wang,[a] Jie Yang,[a] Dacheng Li,[a] Jianmin Dou*[a]*

[a] Shandong Provincial Key Laboratory of Chemical Energy Storage and Novel Cell Technology, College of Chemistry and Chemical Engineering, Liaocheng University, Liaocheng, 252059, P. R. China.

[b] School of Chemistry and Chemical Engineering, Zhoukou Normal University, Zhoukou 466001, P. R. China.

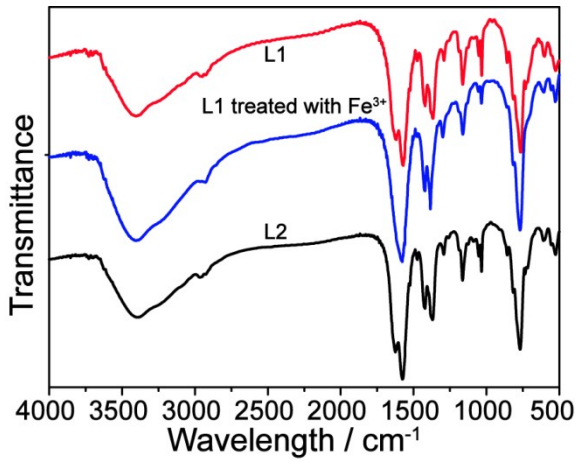

Figure S1. The FT-IR spectra of **L1** before and after treated with Fe^{3+} aqueous, and **L2**.

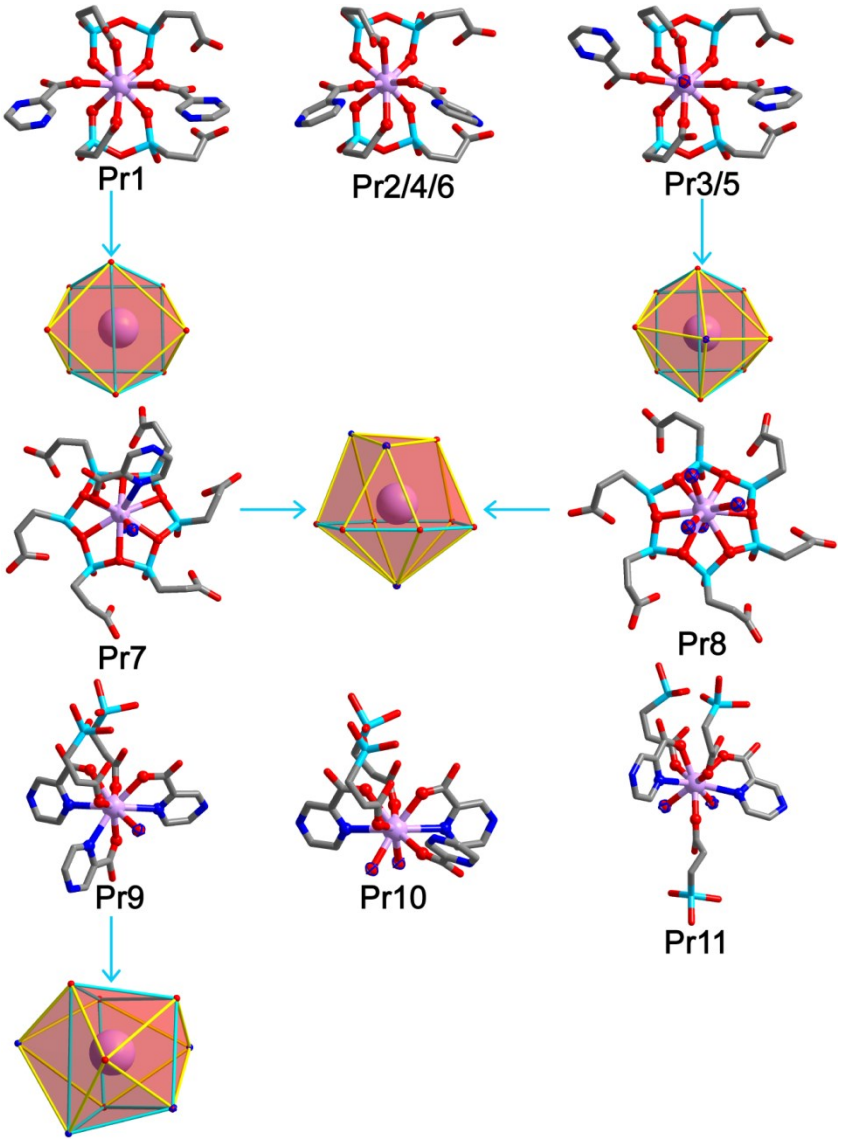

Figure S2. Coordination environments and geometries of Pr^{3+} ions in **L1**.

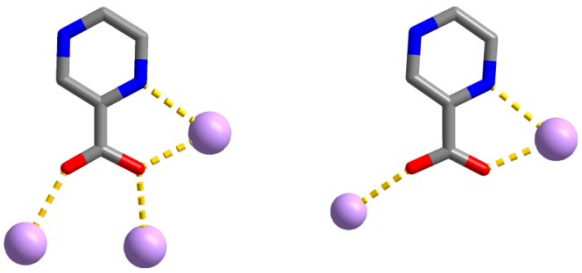

Figure S3. Coordination modes of pza^- ligands in **L1**.

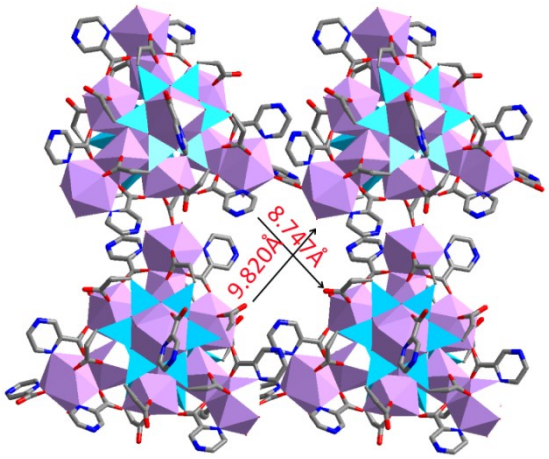

Figure S4. The distorted square window in **L1** with the dimensions of 9.820 × 8.747 $Å^2$.

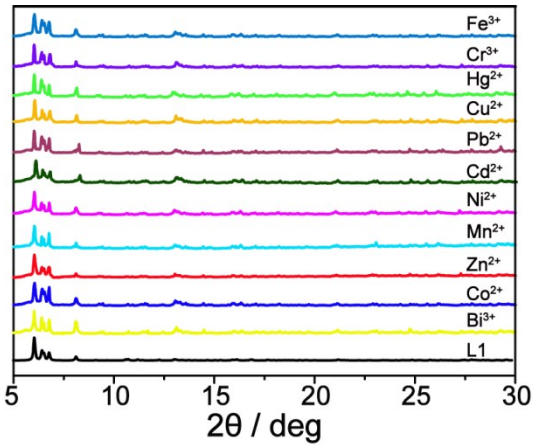

Figure S5. The PXRD patterns of original **L1** and metal-ion-treated **L1**.

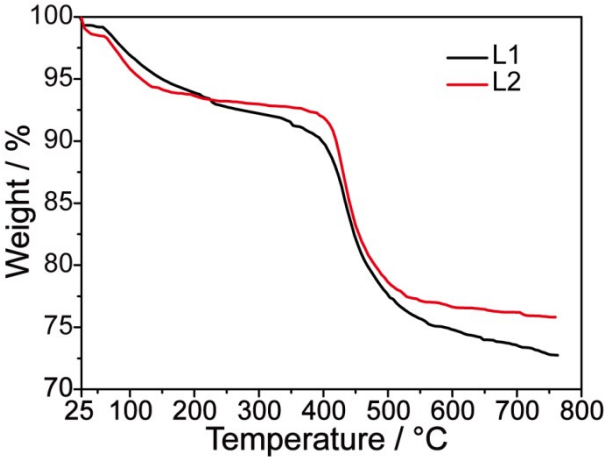

Figure S6. The TGA curves of **L1** and **L2**.

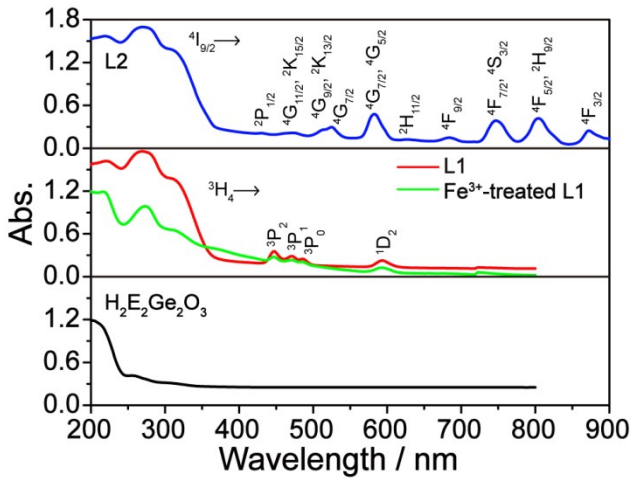

Figure S7. The UV-Vis-NIR absorption spectra of solid $H_2E_2Ge_2O_3$, **L2**, and **L1** before and after treated with Fe^{3+}.

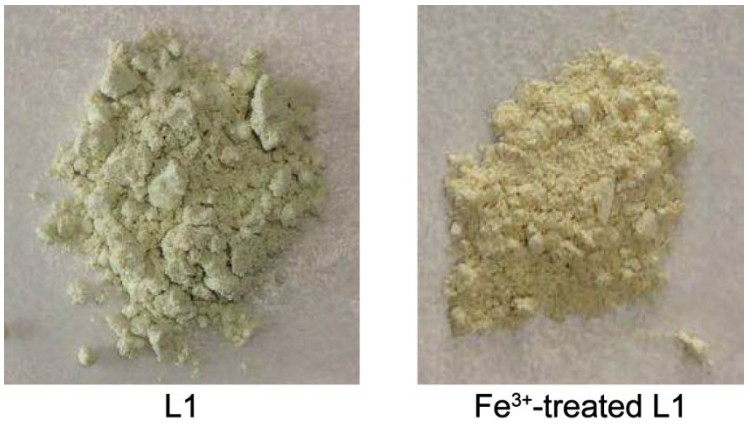

Figure S8. The colours of **L1** and Fe^{3+}-treated **L1**.

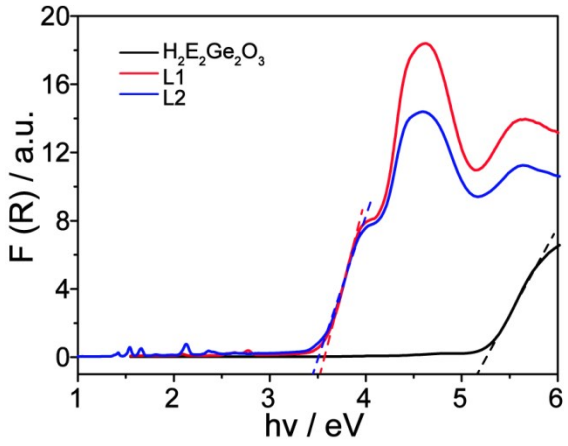

Figure S9. Plots of Kubelka-Munk function of $H_2E_2Ge_2O_3$, **L1** and **L2** band gaps.

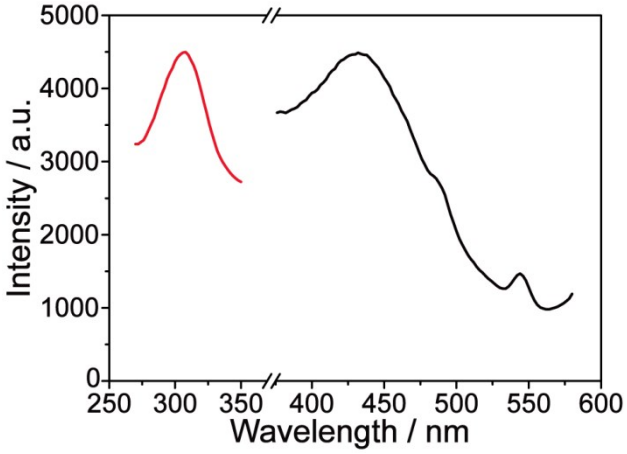

Figure S10. The solid-state excitation (λ_{em} = 434 nm) and emission spectra (λ_{ex} = 307 nm) of $H_2E_2Ge_2O_3$.

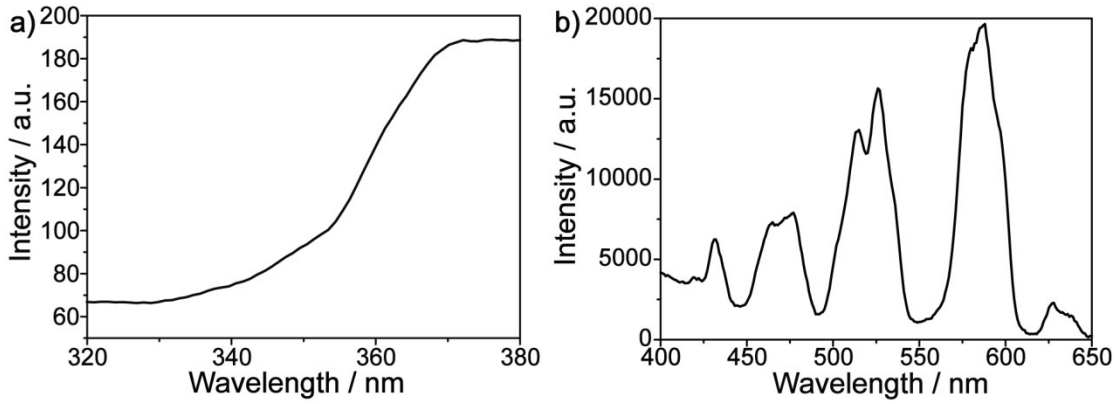

Figure S11. The excitation spectra of **L1** (a) and **L2** (b) (λ_{em}: 420 nm for **L1**; 1063 nm for **L2**).

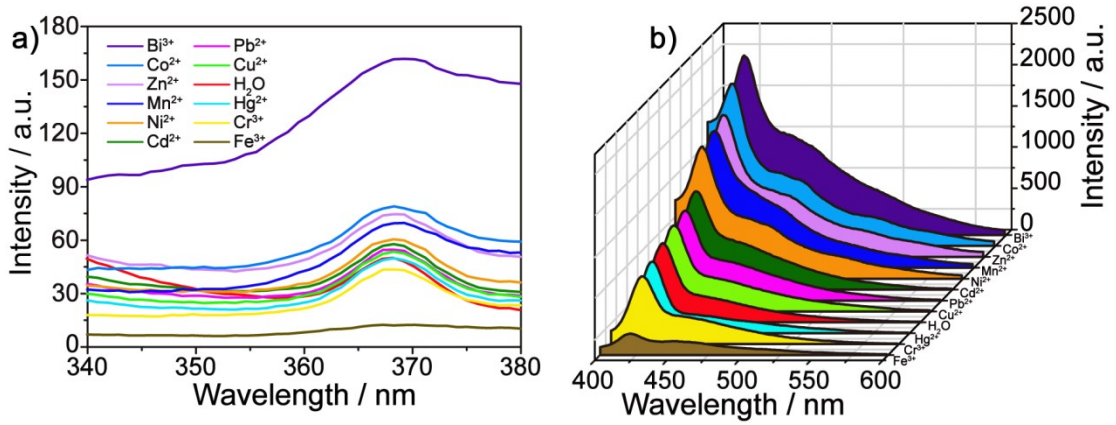

Figure S12. The excitation (a) and emission (b) spectra of **L1** dispersed in aqueous solutions containing different metal ions (λ_{ex} = 368 nm, λ_{em} = 420 nm).

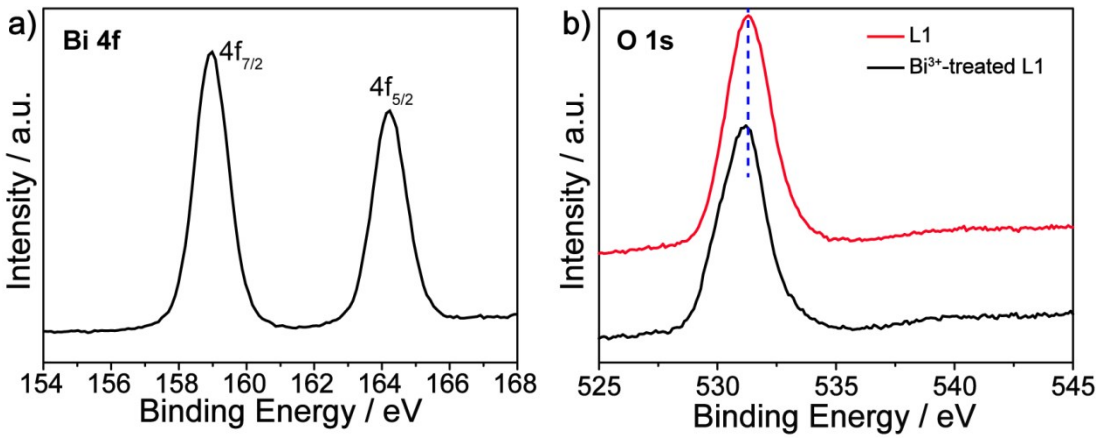

Figure S13. High resolution XPS spectra of Bi 4f and O 1s in Bi^{3+}-treated **L1**.

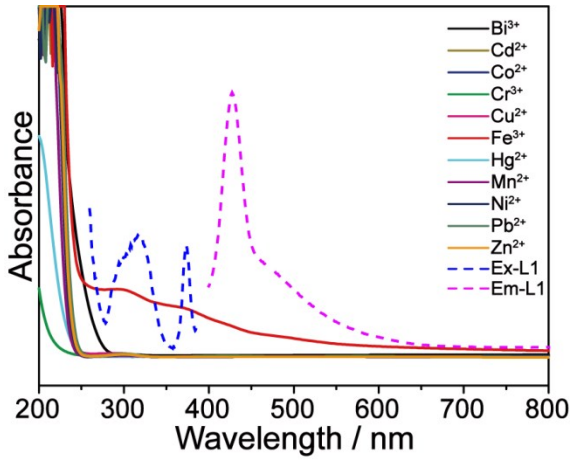

Figure S14. UV-Vis absorption spectra of metal ions in aqueous solutions and excitation and emission spectra of **L1** in water.

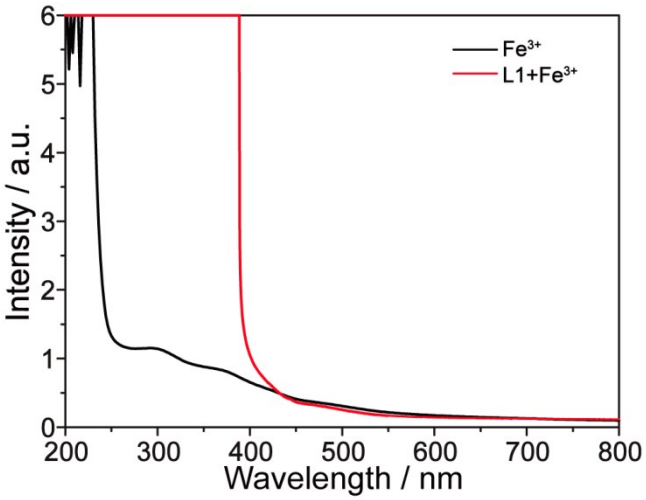

Figure S15. UV-Vis absorption spectra of Fe^{3+} aqueous solution before and after the addition of **L1**.

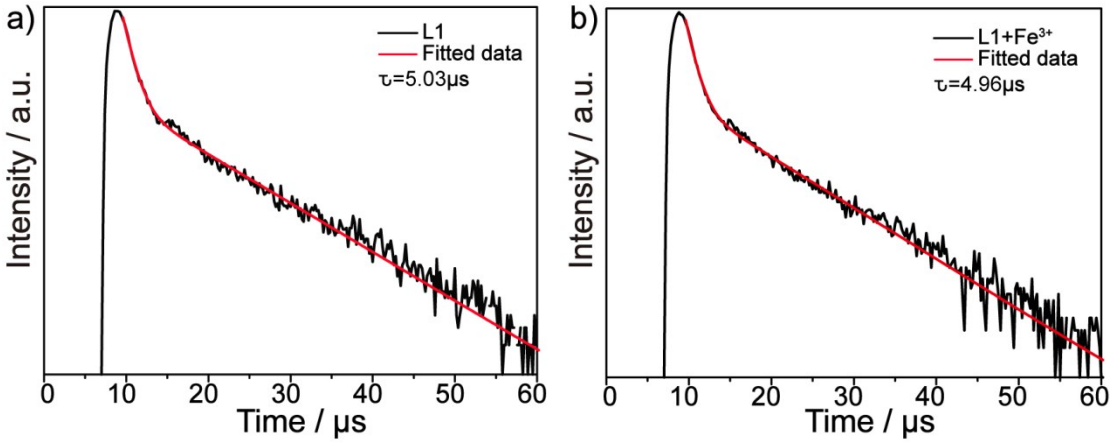

Figure S16. Emission decay curves of **L1** in the absence (a) /presence (b) of Fe^{3+}.

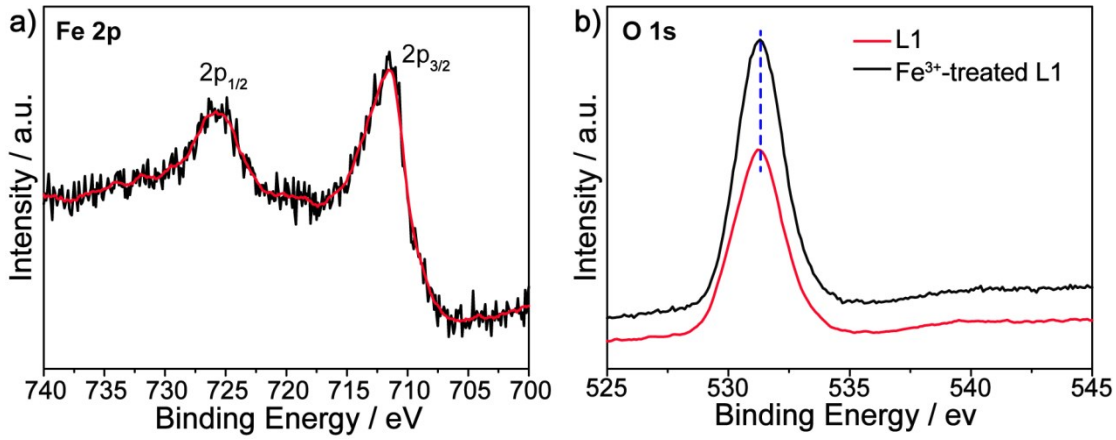

Figure S17. High resolution XPS spectra of Fe 2p (a) and O 1s (b) in **L1** treated with Fe^{3+} aqueous solution.

Table S1. Crystallographic data and structure refinements for **L1** and **L2**.

	L1	**L2**
formula	$C_{76}H_{111}N_{16}O_{84}Ge_{12}Pr_{11}$	$C_{76}H_{111}N_{16}O_{84}Ge_{12}Nd_{11}$
fw	5013.89	4999.47
crystal system	monoclinic	monoclinic
space group	*C*c	*C*c
a, Å	27.515(7)	27.547(5)
b, Å	19.112(5)	19.086(4)
c, Å	27.087(7)	27.056(5)
α, deg	90	90
β, deg	102.745(3)	103.120(2)
γ, deg	90	90
V, Å^3	13893(6)	13854(5)
Z	4	4
D_c, g cm^{-3}	2.397	2.421
F(000)	9536	9580
μ, mm^{-1}	6.433	6.706
Reflections collected/unique	13429/16622	15131/20934
R_{int}	0.0634	0.0501
GOF on F^2	1.007	0.999
R_1, wR_2 (I > 2σ(I))[a]	0.0503, 0.1263	0.0680, 0.1691
R_1, wR_2 (all data)	0.0715, 0.1416	0.1029, 0.1946

Table S2. Standard deviation for **L1**.

Blank Readings	Luminescence Intensity (a.u.)
1	947
2	948
3	938
4	938
5	943
6	939
Standard Deviation (S_b)	4.54